




# Effects of Heat Treatment on the Microstructures and High Temperature Mechanical Properties of Hypereutectic Al–14Si–Cu–Mg Alloy Manufactured by Liquid Phase Sintering Process

Joon-Young Heo<sup>1</sup> · Jin-Han Gwon<sup>2</sup> · Jong-Kwan Park<sup>3</sup> · Kee-Ahn Lee<sup>1</sup> 

Received: 31 July 2017 / Accepted: 5 November 2017 / Published online: 16 March 2018  
© The Korean Institute of Metals and Materials 2018

## Abstract

Hypereutectic Al–Si alloy is an aluminum alloy containing at least 12.6 wt.% Si. It is necessary to evenly control the primary Si particle size and distribution in hypereutectic Al–Si alloy. In order to achieve this, there have been attempts to manufacture hypereutectic Al–Si alloy through a liquid phase sintering. This study investigated the microstructures and high temperature mechanical properties of hypereutectic Al–14Si–Cu–Mg alloy manufactured by liquid phase sintering process and changes in them after T6 heat treatment. Microstructural observation identified large amounts of small primary Si particles evenly distributed in the matrix, and small amounts of various precipitation phases were found in grain interiors and grain boundaries. After T6 heat treatment, the primary Si particle size and shape did not change significantly, but the size and distribution of  $\text{CuAl}_2$  ( $\theta$ ) and  $\text{AlCuMgSi}$  ( $Q$ ) changed. Hardness tests measured 97.36 HV after sintering and 142.5 HV after heat treatment. Compression tests were performed from room temperature to 300 °C. The results represented that yield strength was greater after heat treatment (RT ~ 300 °C: 351 ~ 93 MPa) than after sintering (RT ~ 300 °C: 210 ~ 89 MPa). Fracture surface analysis identified cracks developing mostly along the interface between the primary Si particles and the matrix with some differences among temperature conditions. In addition, brittle fracture mode was found after T6 heat treatment.

**Keywords** Hypereutectic Al–Si · Liquid phase sintering · Microstructure · High temperature mechanical property · T6 heat treatment

## 1 Introduction

Hypereutectic Al–Si alloy is an aluminum alloy containing at least 12.6 wt.% Si. Si particles are distributed throughout the Al matrix in hypereutectic Al–Si alloy, resulting in improved hardness, strength, wear resistance, and low thermal expansion properties. Amidst increasing interest in lightweight materials, hypereutectic Al–Si alloy is gaining great attention from the automotive and aviation industries [1–3]. As aluminum powder metallurgy components are lighter than iron-based powder metallurgy components and have more excellent mechanical properties than aluminum

casted components, many attempts are actively being made to manufacture hypereutectic Al–Si alloy by powder metallurgy [4, 5].

However, manufacturing high quality aluminum components by powder metallurgy is a difficult task. To overcome the difficulties, many studies have been conducted starting from the 1990s, and one solution presented through these studies was the liquid phase sintering process [6, 7]. In the case of aluminum, however, densification through grain boundary diffusion or liquid formation during sintering is hard due to the alumina ( $\text{Al}_2\text{O}_3$ ) oxide layer on the powder's surface. Lumley et al. reported that using Mg will react with the alumina oxide layer, forming a  $\text{MgAl}_2\text{O}_4$  spinel phase as shown in (1), shattering the oxide layer and allowing the liquid within the powder to come out to the grain boundary [6]. Since then, Mg has become a mandatory element in manufacturing aluminum alloys. Furthermore, by decreasing the moisture level in the sintering atmosphere to prevent re-oxidation and by using  $\text{N}_2$  gas, AlN is formed through the

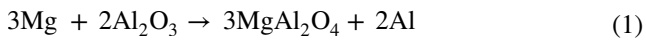
✉ Kee-Ahn Lee  
keeahn@inha.ac.kr

<sup>1</sup> Department of Materials Science and Engineering, Inha University, Incheon 22212, Korea

<sup>2</sup> KORLOY Inc., Cheongju 28589, Korea

<sup>3</sup> Korea Sintered Metal Co. Ltd., Daegu 42983, Korea

reaction (2), attempting to further reduce the wetting angle between the aluminum powder and liquid [8].



Manufacturing hypereutectic Al–Si alloy is also attempted using the above method, and as recent attempts are adding Cu along with Mg as alloying elements to achieve precipitation hardening, the process is becoming more complex, with various byproducts obtained during sintering and increased precipitates from heat treatment. However, current studies about hypereutectic Al–Si alloy manufactured by liquid phase sintering process mostly report about macroscopic microstructure and simple mechanical properties analysis results in accordance with molding pressure and sintering temperature/time/atmosphere [9–11].

Above all, even though hypereutectic Al–Si alloy has the potential of being used in high temperature environments, there are almost no studies reporting the high temperature mechanical properties of the hypereutectic alloy regardless of the types of casting and powder metallurgy processes.

This study investigated the microstructure and room temperature/high temperature mechanical (compression) properties of hypereutectic Al–14Si–Cu–Mg alloy manufactured by liquid phase sintering process, and attempted to analyze the effects of microstructural factors on the deformation and fracture behaviors. In addition, this study also examined the effects of T6 heat treatment on microstructural change and mechanical properties.

## 2 Experimental Methods

The powder used in this study is Alumix 23 from Ecka Granules of Germany, which is an alloy powder with a chemical composition of Al–14Si–2.5Cu–0.5 Mg (wt%). The particle size of the powder used was 40 ~ 80  $\mu\text{m}$ . The powder was molded using 8ton/cm<sup>2</sup> of pressure, and sintering was performed in a high purity N<sub>2</sub> gas (99.999 wt%) atmosphere of 550 ~ 560 °C for 1 h. Dew-point temperature

was controlled and maintained down to – 64 °C. T6 heat treatment applied for precipitation hardening was performed with the following conditions and order: solution heat treatment at 515 °C and water cooling for 1 h, then aging heat treatment at 170 °C, and air cooling. In order to identify the appropriate aging time that achieves the optimum hardness, heat treatment was performed for 0–96 h, and hardness was measured in units of 1 h. The chemical composition analyzed using X-ray fluorescence (XRF) and density measured using the Archimedes method of the manufactured material are listed in Table 1.

To observe and analyze the microstructure of the manufactured material, an optical microscope (OM) from Meiji, scanning electron microscopy (SEM) of Tescan VEGA II LMU, and field emission SEM (FE-SEM) of Tescan LYRA 3 XMH were used. To measure the grain size, primary Si particle size and fraction, pore size, and porosity, the manufactured material was photographed more than 30 times using the OM at  $\times 200$  magnification, and selected images were measured using Image-Analyzer software, and the average of each item was calculated. An X-ray diffraction (XRD) equipment of Rigaku Ultima IV was used for phase analysis under the following conditions: Target: Cu Ka, Angle: 30°–90°, Sampling width: 0.05, Scan speed: 1.0, Power: 35 kV, 20 mA. An electron probe microanalyzer (EPMA) of Shimadzu EPMA-1600 was used for element distribution analysis.

Hardness was measured 10 times using Vickers hardness tester of AVK-C100 with these load conditions: 0.5 kgf, measurement scale:  $\times 100$  and minimum reading: 0.1  $\mu\text{m}$ , and the average of the measurements was calculated and used. To identify room temperature and high temperature mechanical properties, a compression test was performed. The specimen used for the test was a cylindrical specimen 4 mm in diameter and 6 mm in length, and the test conditions were room temperature, 200, 250 and 300 °C, with a strain rate of 10<sup>–3</sup> s<sup>–1</sup> achieved using MTS-810 equipment. To examine the deformation and fracture behaviors at each temperature after the compression test, the surface and fracture surface of the compression specimen were observed using SEM and FE-SEM.

**Table 1** Chemical composition and density analysis results of the hypereutectic Al–Si alloy used in this study

wt%	Al	Si	Cu	Mg
Std. (powder)	Bal.	14	2.5	0.5
Alloy	Bal.	15.45	2.82	0.49
Green density	Sintered density		Theoretical density	
2.45 g/cm <sup>3</sup>	2.61 g/cm <sup>3</sup>		2.68 g/cm <sup>3</sup>	
			Relative density	
			97.22%	

### 3 Results and Discussion

#### 3.1 Hardness Variation Depending on Aging Heat Treatment Time

Figure 1 shows the Vickers hardness change at 170 °C depending on aging heat treatment time. The hardness decreases slightly at the early stage of heat treatment, then increases over time, and achieves maximum hardness in the 6- to 12-h range. Such is very similar to the aging behavior of Al 2xxx (Al–Cu, Al–Cu–Mg) and Al 6xxx (Al–Mg–Si) alloys which have a precipitation hardening

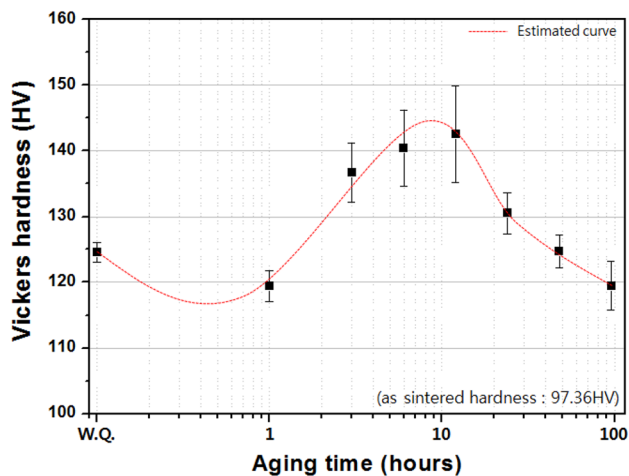


**Fig. 1** Hardness variation results in accordance with aging time of hypereutectic Al–Si alloy at 170 °C

effect [12]. However, the hardness slightly decreasing in initial heat treatment is a phenomenon which occurs in certain aluminum alloys and at certain aging heat treatment temperatures. Some studies suggest that alloy elements undergoing solid solution strengthening in a supersaturated solid solution condition are used in the initial precipitation phase formation, causing the solid solution strengthening to decrease [13]. Based on such results, this study observed the microstructure and investigated the high temperature mechanical properties of the specimen obtained after sintering (as sintered) and the specimen with the maximum hardness obtained after 12 h of heat treatment (T6 heat treated).

#### 3.2 Microstructures of Al–14Si–Cu–Mg Alloys

Figure 2 shows the OM ( $\times 100, \times 200$ ) observation results of microstructures of the as sintered and T6 heat treated specimens. Figure 2a is the as sintered and Fig. 2b is the T6 heat treated, and both specimens show round, dark-colored primary Si particles distributed on a bright Al matrix. In order to identify the difference generated by heat treatment, the OM images were analyzed for quantitative measurement of microstructural characteristics, and the results are listed in Table 2. The primary Si particle size was 8–9  $\mu\text{m}$ , fraction was 20% and distribution was relatively even compared to that of conventional casting process [14]. The porosity was less than 0.7%, which is an evidence that hypereutectic Al–Si alloy manufactured by liquid phase sintering process is a high density material (refer to Table 1). After heat treatment, the grain size, primary Si particle size and fraction increased slightly, while pore size and porosity decreased slightly.

**Fig. 2** Microstructural observation Results of as-sintered (a) and T6 heat treated (b) hypereutectic Al–14Si–Cu–Mg alloys

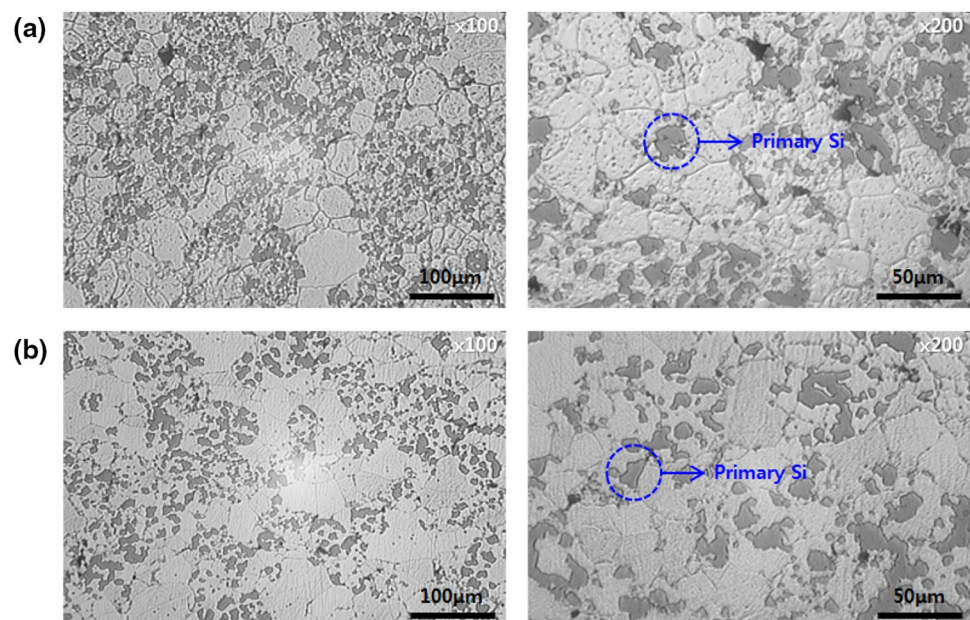


**Table 2** Summary of microstructural characteristics of hypereutectic Al–14Si–Cu–Mg alloys identified from Fig. 2: grain size, primary Si size, fraction of primary Si, pore size and porosity

	Grain size ( $\mu\text{m}$ )	Primary Si size ( $\mu\text{m}$ )	Fraction of Primary Si (%)	Pore size ( $\mu\text{m}$ )	Porosity (%)
As sintered	21.02 ( $\pm 10.6$ )	8.24 ( $\pm 7.3$ )	20.4	8.05 ( $\pm 4.4$ )	0.66
T6 heat treated	23.16 ( $\pm 12.4$ )	8.95 ( $\pm 6.5$ )	20.7	7.31 ( $\pm 5.6$ )	0.62

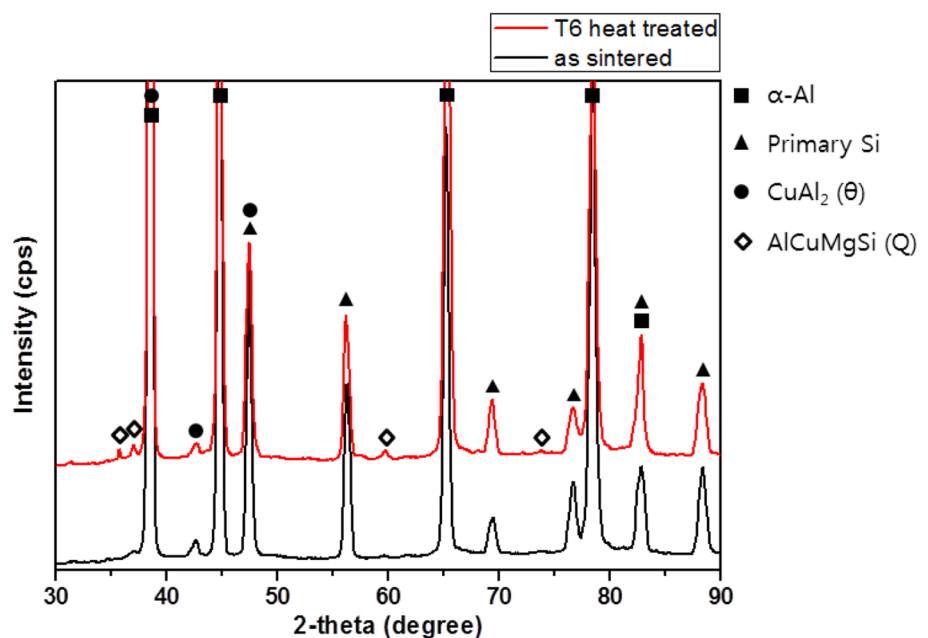
In the case of hypereutectic Al–Si alloy manufactured by simple casting process, the primary Si particle is an angular shape and very rough and large as its size is greater than  $50\ \mu\text{m}$  [14]. So in order to refine the primary Si particle size, new casting processes such as thixoforming, lost foam, squeeze casting, electromagnetic stirring, etc. are frequently attempted and used. Though such processes primary Si particle size can be decreased to some extent, but there are limits to primary Si particle fraction increase and even distribution of primary Si particle [15]. Therefore, the even microstructural control of fine ( $8\text{--}9\ \mu\text{m}$ ) primary Si phases achieved by this study using the liquid phase sintering process can be deemed as a significant achievement.

Figure 3 shows the XRD phase analysis results. Basically the as sintered and T6 heat treated specimens are both composed of  $\alpha\text{-Al}$ , primary Si and  $\text{CuAl}_2$  ( $\theta$ ), and  $\text{AlCuMgSi}$  ( $Q$ ) was shown clearly along with the aforementioned after heat treatment. The precipitation phases commonly reported to be found in Al–Si–Cu–Mg based alloys are  $\text{CuAl}_2$  ( $\theta$ ),  $\text{Al}_2\text{CuMg}$  ( $S$ ) and  $\text{Mg}_2\text{Si}$  ( $\beta$ ). In the case of  $\text{AlCuMgSi}$  ( $Q$ ), it is formed during solution heat treatment of Al–Cu–Mg based alloys with Si content of 0.5 wt.% or more, and it is reported to support the formation of  $\text{CuAl}_2$  ( $\theta$ ) phase

by reducing Mg content in the matrix rather than forming  $\text{Al}_2\text{CuMg}$  ( $S$ ) and  $\text{Mg}_2\text{Si}$  ( $\beta$ ) [15, 16].

EPMA analysis was performed to identify the shape and distribution of phases, and the results are indicated in Fig. 4. The common characteristics found in the element distribution map of the as sintered (Fig. 4a) and T6 heat treated (Fig. 4b) specimens are that primary Si particles are present in the Al matrix and Al–Mg based oxides are distributed along the grain boundary. The difference between the two specimens is that Cu element in the as sintered specimen are irregular and non-continuous, while Cu element in the T6 heat treated specimen is generally evenly distributed and is found together with Al, Si and Mg elements in the grain boundary.

In order make a more detailed analysis, FE-SEM high magnification observation was performed, and the results are shown in Fig. 5. The low magnification ( $\times 5\ \text{k}$ ) image of the as sintered specimen in Fig. 5a shows white and light grey phases partially present in the grain boundary. EDS analysis confirmed that the white particles are  $\text{CuAl}_2$  ( $\theta$ ), and the light grey phase is  $\text{AlCuMgSi}$  ( $Q$ ). Meanwhile, the high magnification ( $\times 30\ \text{k}$ ) image of Fig. 5a shows a relatively massive, approximately  $0.5\ \mu\text{m}$  sized,  $\text{CuAl}_2$  ( $\theta$ ) present in

**Fig. 3** XRD analysis results of as-sintered and T6 heat treated hypereutectic Al–Si alloys



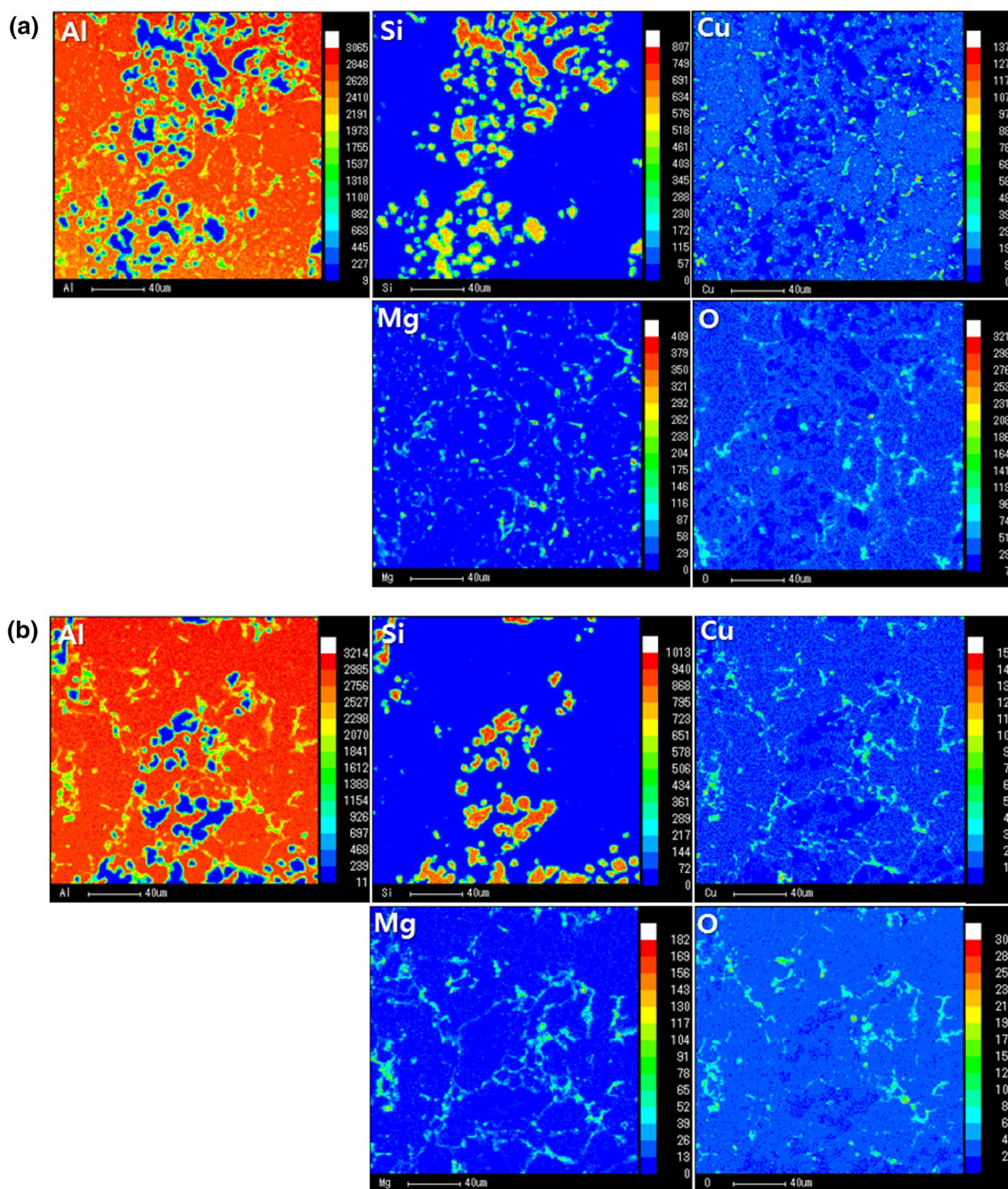


**Fig. 4** EPMA analysis results of as-sintered (a) and T6 heat treated (b) hypereutectic Al–Si alloys

the grain interior. The low magnification ( $\times 5$  k) image of the T6 heat treated specimen in Fig. 5b shows large amounts of light grey  $\text{AlCuMgSi}$  ( $Q$ ) in the grain boundary mixed with white  $\text{CuAl}_2$  ( $\theta$ ). The high magnification ( $\times 30$  k) image of the T6 heat treated specimen (Fig. 5b) shows tens of sub-nanometer-sized  $\text{CuAl}_2$  ( $\theta$ ) evenly distributed in the grain interior [17].

The hypereutectic Al–14Si–Cu–Mg alloy in this study is an alloy designed to achieve strengthening effect of primary

Si particle by adding Cu along with Si and to achieve precipitation hardening through Cu. Therefore, as T6 heat treatment is applied, the precipitation process of supersaturated solid solution  $\rightarrow$  GP zone  $\rightarrow$   $\theta''$   $\rightarrow$   $\theta'$   $\rightarrow$   $\theta$  takes place, which possibly can be assumed to trigger fine re-precipitation and redistribution of  $\text{CuAl}_2$  ( $\theta$ ). In the case of  $\text{AlCuMgSi}$  ( $Q$ ), it is assumed to be formed from the Mg element added to induce reaction (1), and as it was formed in the grain boundary in a large amount after T6 heat treatment, it is required

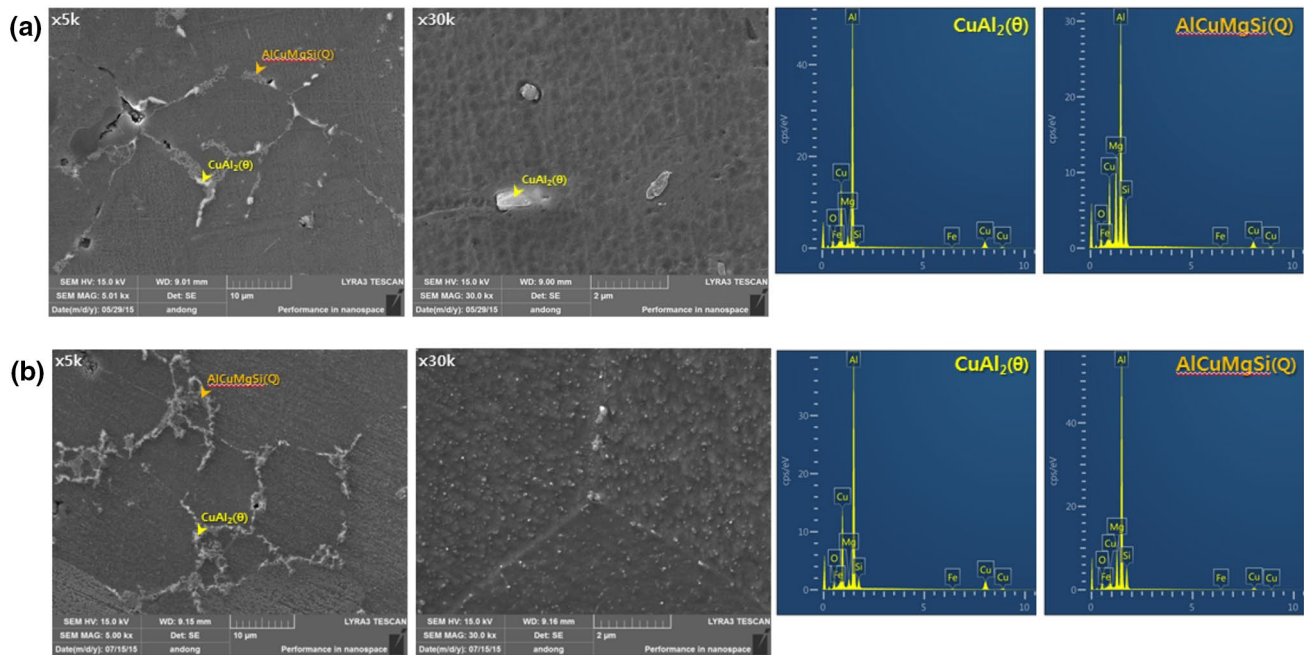


**Fig. 5** FEM and EDS analysis results of as-sintered (a) and T6 heat treated (b) hypereutectic Al-Si alloys

to further investigate about the effects of AlCuMgSi (Q) on the mechanical properties of the manufactured material. Meanwhile, the Al-Mg based oxide identified in the EPMA element distribution map in Fig. 4 was not found at all in the FE-SEM image in Fig. 5. It is assumed that the Al-Mg based oxides are a byproduct of reaction (1) but formed in an extremely thin film mixed with other phases, causing it to possibly be present discontinuously throughout the material, which makes it difficult to observe even with FE-SEM.

### 3.3 Room and High Temperature Mechanical Properties

Figure 6 shows the results of a room temperature Vickers hardness test of the as sintered and T6 heat treated specimens. The as sintered specimen measured 97.36 HV and the T6 heat treated specimen measured 142.5 HV, showing a 1.5 times hardness increase after heat treatment. Although there are some differences among alloys, the hardness increase effect through T6 heat treatment is generally known to be approximately 1.2–2.0 times. Therefore, in order for a precipitation strengthened aluminum alloy to have outstanding hardness, the hardness prior to heat treatment must be sufficiently high. Considering that the hardness of the T6 heat treated commercial aluminum ranges from 50 to 140 HV, it is possible to know that the as sintered specimen in this study has a relatively high hardness.

The hardness of cast hypereutectic Al-Si alloy with Si content of 14 wt.% or less is reported as 77–98 HV,

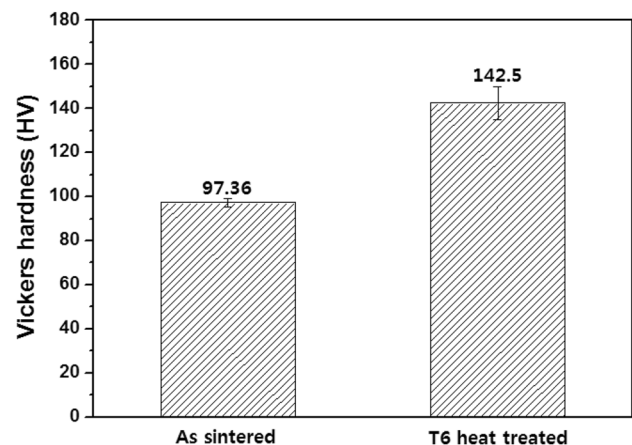


**Fig. 6** Vickers hardness results of as-sintered and T6 heat treated hypereutectic Al-Si alloys

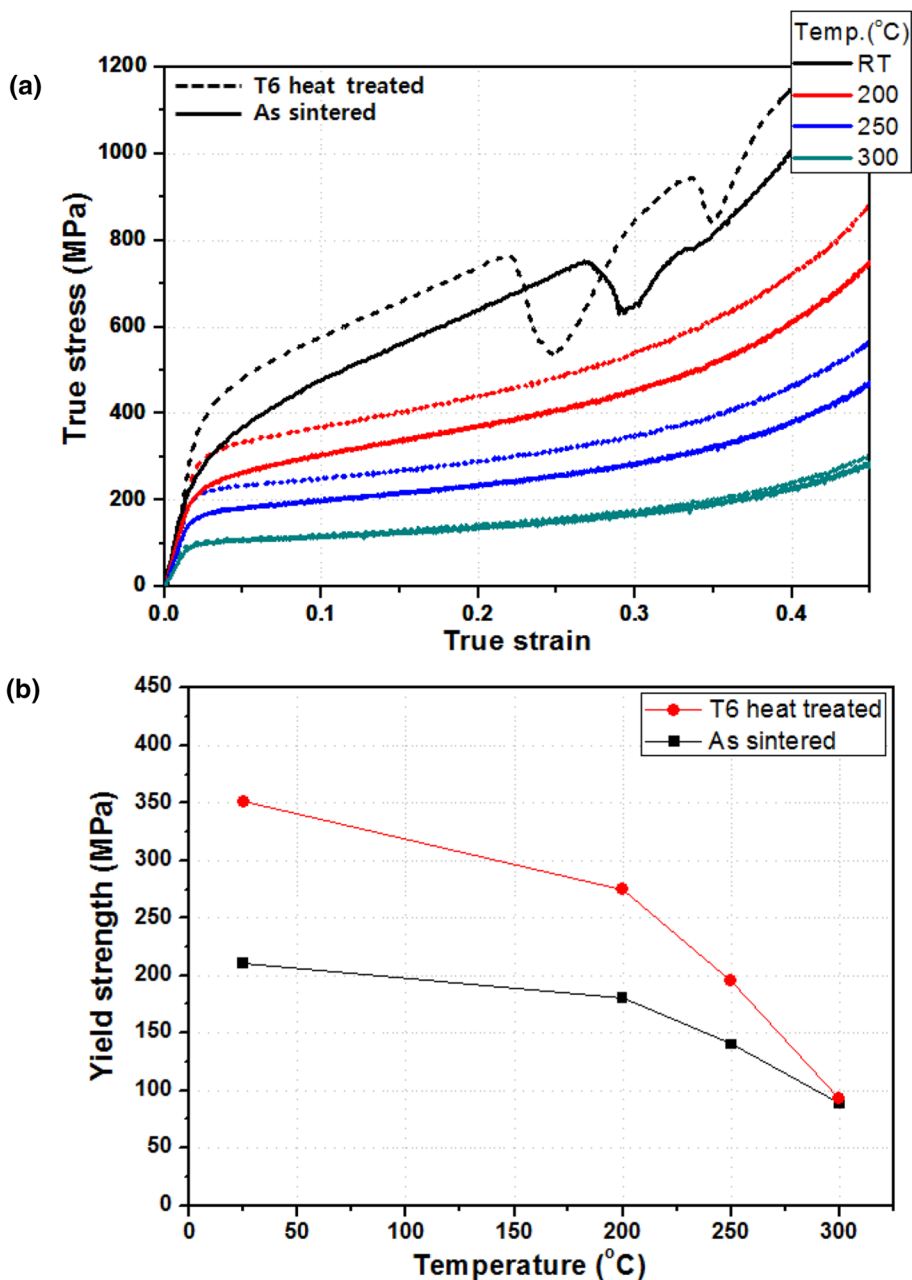
and with Si content of 20 wt.% or more is reported as 141–163 HV. Even though the Si content of the hypereutectic Al-Si alloy in this study is only 14 wt.%, its hardness measured nearly up to the level of Al-20 wt.% Si cast alloy. This means that the strengthening of hardness of Al-Si alloys is influenced not only by the Si content but also by the primary Si particle size and fraction. The hypereutectic Al-Si alloy manufactured by powder metallurgy (liquid sintering) in this study is suspected to achieve outstanding hardness due to the fine primary Si particle

relative to its Si content, high fraction, even distribution and the additional strengthening phase,  $\text{CuAl}_2$  ( $\theta$ ).

Figure 7 shows the room and high temperature compression results. The compressive stress–strain curves in Fig. 7a measured room temperature yield strength of 210 MPa for the as sintered specimen and 351 MPa for the T6 heat treated specimen. The room temperature strength increase after T6 heat treatment showed a similar trend as that of the hardness increase. The room temperature compression curve showed work hardening after yield point, and the fracture strain when initial fracture (stress decreases drastically) occurs was measured as 0.30 for the as sintered specimen and 0.23 for the T6 heat treated specimen, which can be interpreted that

the ductility of the material decreased after T6 heat treatment. The high temperature (200–300 °C) compression tests resulted in no fractures, unlike the room temperature condition, and compressive deformation occurred continuously until the set strain ( $\epsilon_f=0.45$ ). A normal trend of strength decreasing as well as elastic zone and work hardening zone slopes decreasing as temperature increased was confirmed. Figure 7b shows the yield strength depending on temperature measured 200 °C: 181 MPa, 250 °C: 140 MPa and 300 °C: 89 MPa for the as sintered specimen, and 200 °C: 275 MPa, 250 °C: 195 MPa and 300 °C: 93 MPa for the T6 heat treated specimen. The yield strength of the T6 heat treated specimen is greater at all temperature conditions than the as sintered

**Fig. 7** Room and high temperature compression curves with temperature (a) and yield strengths with temperature (b) of as-sintered and T6 heat treated hypereutectic Al–Si alloys





specimen. However, the strength difference remains large until 250 °C, and at 300 °C, the strength becomes nearly similar.

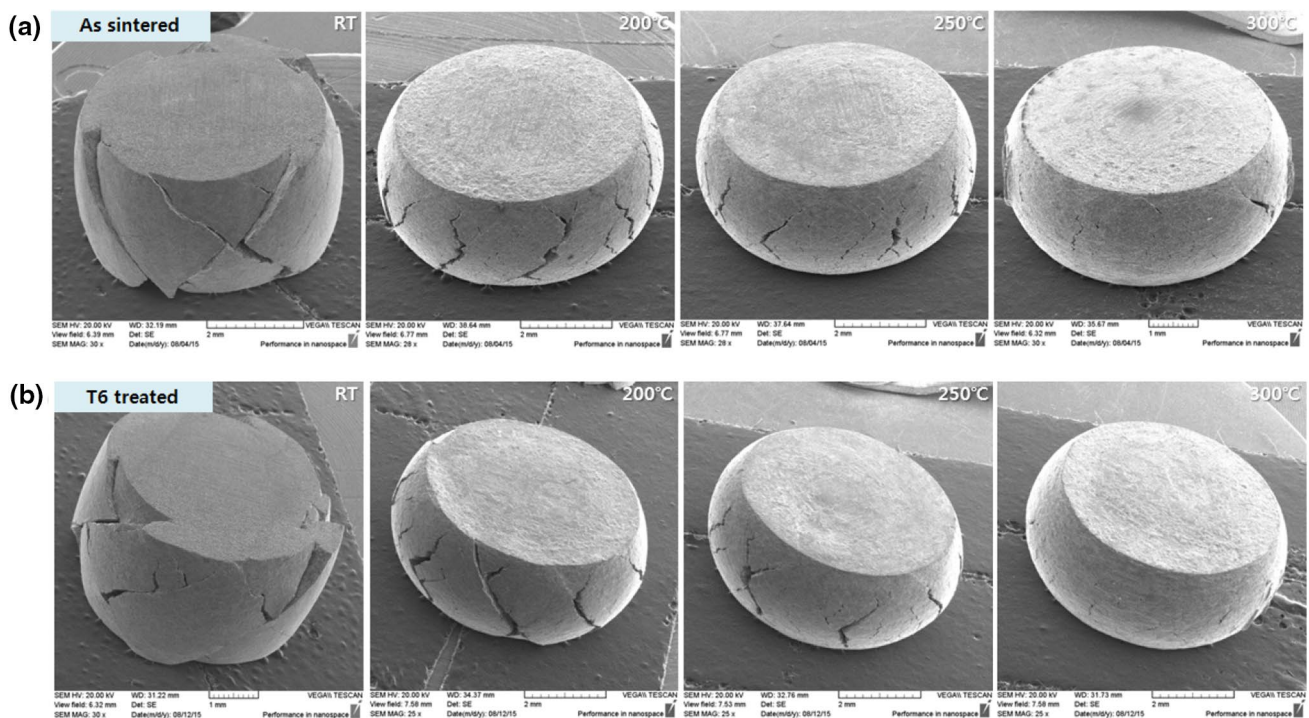
### 3.4 Deformation and Fracture Behaviors

Figure 8 shows the macroscopic observation results of the high temperature compressed specimens of the as sintered and the T6 heat treated ones. The as sintered specimen in Fig. 8a and the T6 heat treated specimen in Fig. 8b both show similar trends in all temperature conditions. The first thing to note is the massive fracture crack formed from the top to the bottom of the specimen especially at room temperature. This crack can be interpreted in relation to the apparent fluctuation phenomena that occurred in the room temperature compression curves in Fig. 7a. On the other hand, starting from 200 °C, a large number of macro shear cracks were formed on the surface rather than a fracture crack on the whole specimen. The surface cracks decreased as temperature increased, and at 300 °C, there were nearly no surface cracks.

Figure 9 shows high magnification observation results of the typical surface rather than the massive fracture crack area of the compression specimen. Unlike the results in Fig. 8, the as sintered specimen and the T6 heat treated specimen showed a little different trends. From room temperature to 300 °C, a large amount of fine, irregular-shaped shear

cracks were formed on the specimen surface. These macro shear cracks increased in number and developed further as temperature increased. The as sintered specimen shown in Fig. 9a and the T6 heat treated shown in Fig. 9b do not have significant differences at room temperature, but starting from 200 °C, the number of cracks was smaller in the T6 heat treated specimen than in the as sintered specimen. Meanwhile, aside from the shear cracks in the near 45° direction, there were a number of fine vertical cracks, and these cracks did not show a significant difference among specimens or temperature conditions.

Through the form and size of the cracks formed on the specimen after the compression test, the material's deformation and fracture behaviors can be discussed. In general, the shear cracks formed on the compression specimen surface are a phenomenon occurring in relatively hard steel materials (hot-worked/cold-worked material, precipitation/dispersion strengthened material, etc.). Compressive deformation causes phenomena such as an increase in dislocation density and dynamic recrystallization, and if the structure fails to sufficiently accommodate the deformation, shear bands or shear cracks of 45° are formed. Shear cracks start from fine cracks, and spread drastically as local coarse cracks. This process is similar to that of the fracture process after deformation, which allows the fine cracks to be suspected to be caused by deformation and massive cracks to be caused by fracturing [18]. Therefore, as in Figs. 8 and 9, the increase/



**Fig. 8** Macroscopic observation results of high temperature compressed specimens of as-sintered (a) and T6 heat treated (b) hypereutectic Al-Si alloys with deformation temperature



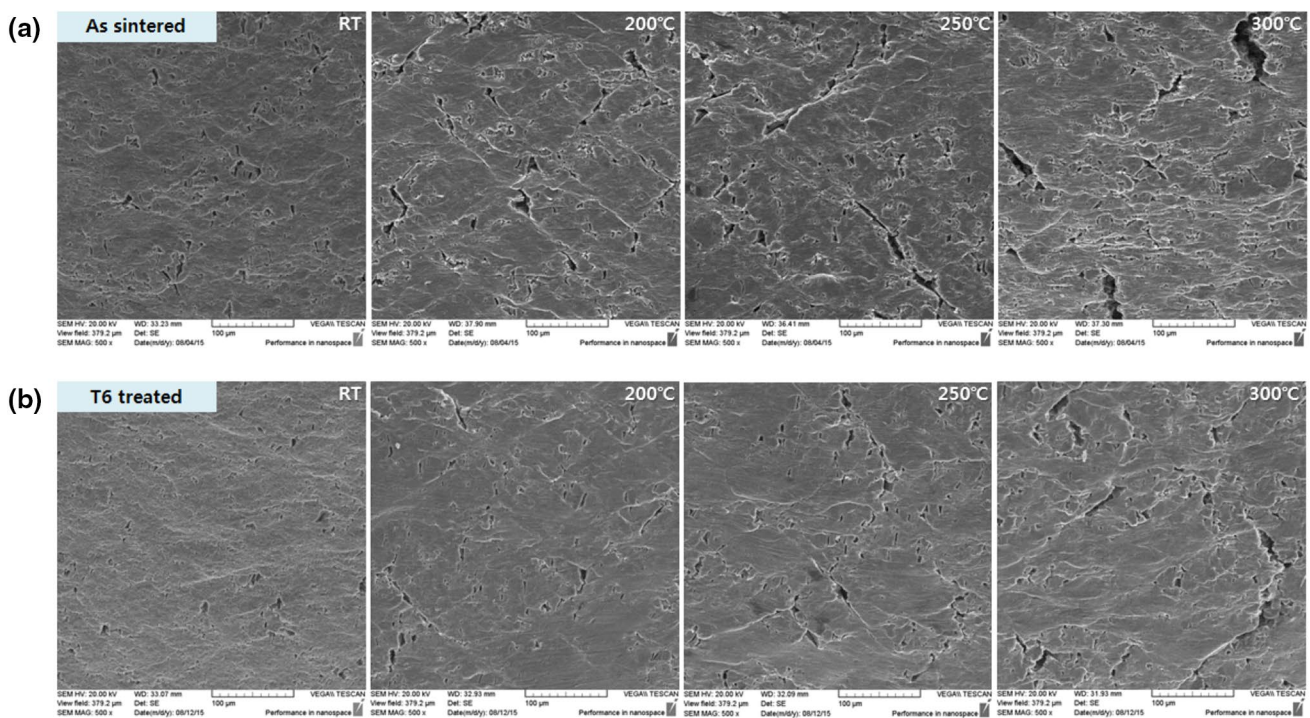


**Fig. 9** Microscopic surface observation results of high temperature compressed specimens of as-sintered (a) and T6 heat treated (b) hypereutectic Al–Si alloys with deformation temperature

decrease of the number of fine or massive shear cracks can be interpreted to be the same phenomenon as the deformation being more likely and fracture being suppressed as temperature increases. Also, the reason why there are fewer micro shear cracks in the compression specimen than in the as sintered specimen from 200 °C is suspected to be caused by the suppression of deformation due to the fine re-precipitation and redistribution of fine  $\text{CuAl}_2$  ( $\theta$ ) after T6 heat treatment.

Figure 10 shows the FE-SEM high magnification observation results of the fracture surface inside massive crack area of the room temperature and 200 °C compressed test specimens. The as sintered specimen shown in Fig. 10a features active elongation and deformation accommodation of the Al matrix around the angular-shaped primary Si particles. Also, some primary Si particles were identified to be shattered (yellow arrows). The T6 heat treated compression test specimen shown in Fig. 10b features primary Si particles and fine particles assumed to be  $\text{CuAl}_2$  ( $\theta$ ) and  $\text{AlCuMgSi}$  ( $Q$ ) distributed throughout the fracture surface, which indicate decreased elongation of the Al matrix. Shattered primary Si particles (yellow arrows) were also identified in this specimen as well.

In order to observe the conditions of the Al matrix and primary Si particle after compression deformation, the fracture surface inside massive crack area of the room temperature compressed specimen was observed with high

magnification, and the result is shown in Fig. 11. The Al matrix and primary Si particle have an incoherent interface, and this interface between phases can separate during deformation from a composite material perspective. However, as shown in Fig. 11a, b, the manufactured materials maintained their adherence between the Al matrix and primary Si particle on the fracture surface of the as sintered and T6 heat treated compression specimens. The shattered primary Si particles on the fracture surface indicate that the primary Si particles are enough and performing as an effective strengthening phase. The reason why the stress level can increase up to the point where primary Si particles would shatter is because the Al matrix and primary Si particles have the outstanding interface adherence between phases. In relation to the aforementioned, the cause of the formation of fine vertical cracks in Fig. 9 can be judged to be due to the shattering of primary Si particles.

## 4 Conclusions

This study investigated the microstructure and high temperature mechanical properties of hypereutectic Al–14Si–Cu–Mg alloy manufactured by liquid phase sintering process, and came to the following conclusions:

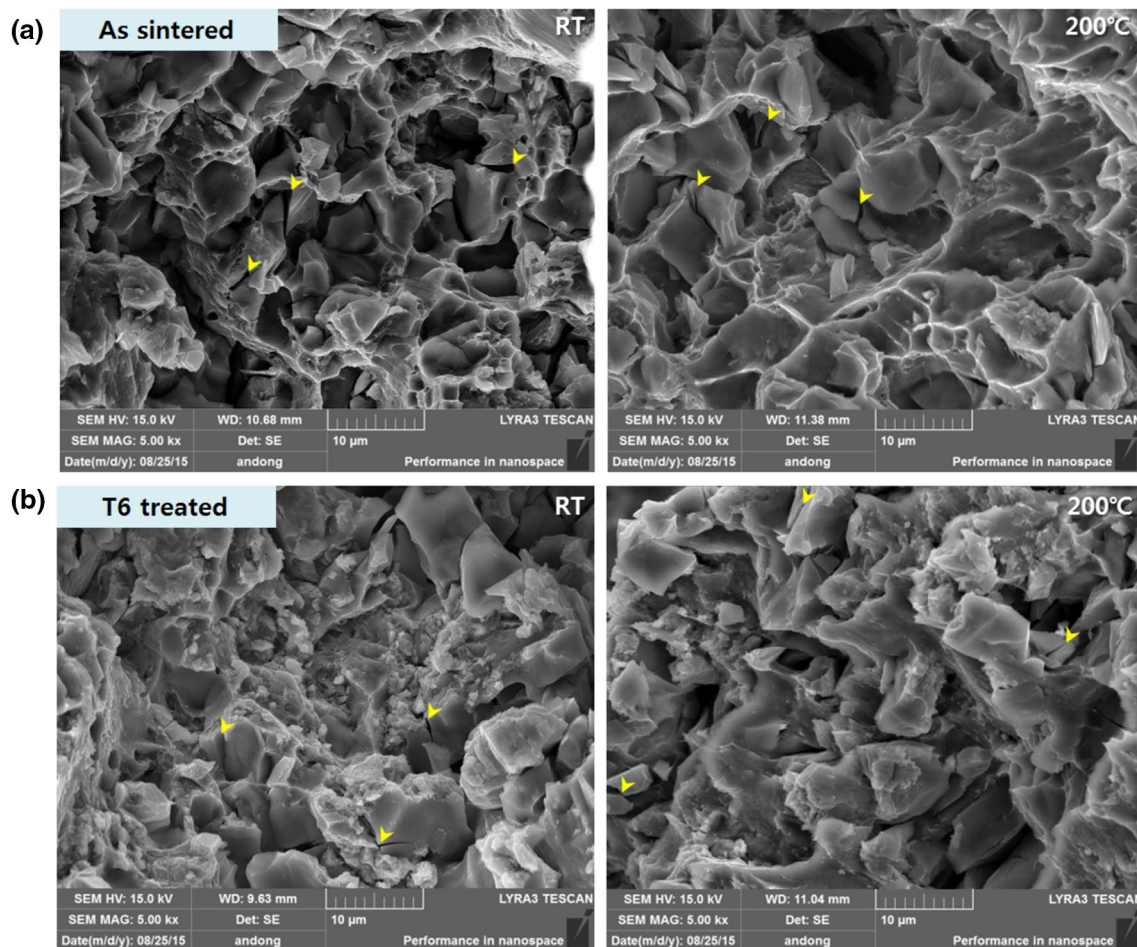
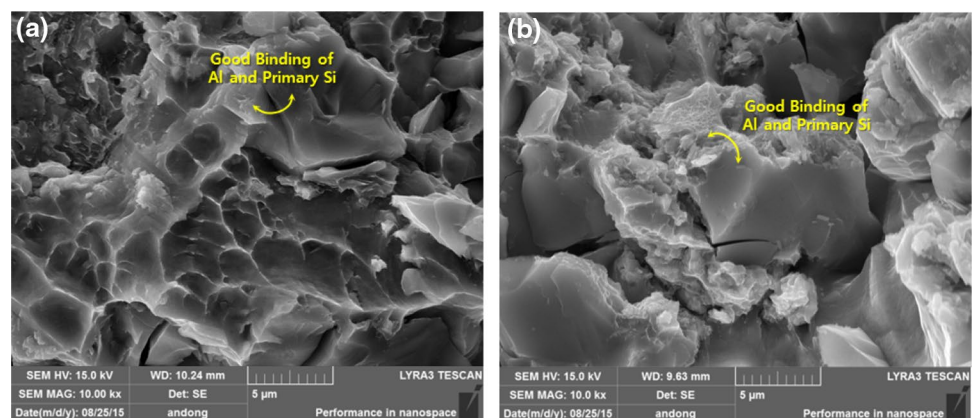


**Fig. 10** FE-SEM observation results of fracture surfaces inside massive cracks of room temperature and 200 °C compressed specimens

**Fig. 11** High Magnification FE-SEM observation results of fracture surfaces inside massive cracks of room temperature compressed specimens of as-sintered (a) and T6 heat treated (b) hypereutectic Al–Si alloys



1. After observing the microstructures of specimens right after sintering and heat treatment, the primary Si particle size was small (8–9  $\mu\text{m}$ ), fraction was at about 20%, and the distribution was relatively even. The relative density was 97.22% and porosity measured at less than 0.7%, confirming that the manufactured material is a high density material. No significant change was found in the

primary Si particle before and after T6 heat treatment, and large amounts of fine re-precipitation and redistribution of  $\text{CuAl}_2(\theta)$  as well as  $\text{AlCuMgSi}(Q)$  were found to be formed in a large amount in the grain boundary.

2. The Vickers hardness test measured 97.36 HV after sintering and 142.5 HV after heat treatment, showing an increase of approximately 1.5 times after T6 heat

treatment. The room temperature and high temperature compression tests confirmed higher yield strength after heat treatment (RT ~ 300 °C: 351–93 MPa) than after sintering (RT ~ 300 °C: 210–89 MPa). The hardness difference before and after heat treatment was large up to 250 °C, and the hardness became nearly identical in the 300 °C condition.

3. The observation results of compression specimens confirmed that coarse shear cracks and micro shear cracks were formed. The number of massive cracks decreased and micro shear cracks increased as temperature increased. Starting from 200 °C, the number of micro shear cracks in the heat treated compression specimen was smaller than the compression specimen after sintering. Observation of the fracture surface inside massive cracks identified active elongation and deformation accommodation in the compression specimen after sintering. The compression specimen after heat treatment featured fine particles, suspected to be  $\text{CuAl}_2$  ( $\theta$ ) and  $\text{AlCuMgSi}$  ( $Q$ ), distributed throughout the fracture surface, which caused the elongation of the Al matrix to decrease significantly. In all specimens, shattered primary Si particles were observed before and after heat treatment.
4. Hypereutectic Al–14Si–Cu–Mg alloy manufactured by liquid phase sintering process has primary Si particles with the most ideal size, fraction and distribution, and the high interface adherence between the Al matrix and Si phase is suspected to contribute to the outstanding mechanical properties of the alloy. The fine re-precipitation and redistribution of  $\text{CuAl}_2$  ( $\theta$ ) after T6 heat treatment also contribute to the improved hardness and strength.

## References

1. I.P. Melashenko, Powder Metall. Met. Ceram. **27**, 790 (1987)
2. G.B. Schaffer, T.B. Sercombe, R.L. Lumley, Mater. Chem. Phys. **67**, 85 (2001)
3. T. Pieczonka, Th Schubbert, S. Baunack, B. Kieback, J. Mater. Sci. Eng A **478**, 251 (2008)
4. P. Delarbre, M. Krehl, in *Int. Conf. on P/M Aluminum and Light Alloys for Automotive Applications*, Detroit (2000)
5. *Aluminum Industry Roadmap for the Automotive Market*, The Aluminum Association Inc. (1999)
6. R.N. Lumley, T.B. Sercombe, G.B. Schaffer, Metall. Mater. Trans. A **30**, 457 (1999)
7. T.B. Sercombe, G.B. Schaffer, Acta Mater. **52**, 3019 (2004)
8. T.B. Schaffer, B.J. Hall, S.J. Bonner, S.H. Huo, T.B. Sercombe, Acta Mater. **54**, 131 (2006)
9. D.W. Heard, I.W. Donaldson, D.P. Bishop, J. Mater. Process. Technol. **209**, 5902 (2009)
10. H. Rudianto, S.S. Yang, K.W. Nam, Y.J. Kim, Rev. Adv. Mater. Sci. **28**, 145 (2011)
11. S.S. Su, I.T.H. Chang, W.C.H. Kuo, Mater. Chem. Phys. **139**, 775 (2013)
12. W.F. Smith, *Structure and Properties of Engineering Alloys* (McGraw-Hill, New York, 1993)
13. M.J. Starink, V.M.F. Abeels, P. van Mourik, Mater. Sci. Eng., A **163**, 115 (1993)
14. L. Lasa, J.M. Rodriguez-Ibabe, Mater. Sci. Eng., A **363**, 193 (2003)
15. L. Lasa, J.M. Rodriguez-Ibabe, J. Mater. Sci. **39**, 1343 (2004)
16. R.M. Gomesm, T. Sato, H. Tezuka, A. Kamio, Mater. Trans. **39**, 357 (1998)
17. G.S. Ham, M.S. Baek, J.H. Kim, S.W. Lee, K.A. Lee, Met. Mater. Int. **23**, 35 (2017)
18. T. Sakai, A. Belyakov, R. Kaibyshev, H. Miura, J.J. Jonas, Prog. Mater. Sci. **60**, 130 (2014)